# Complex but negligible: non-linearity of the inertial coupling between the platform and blades of floating wind turbines

Richard C Lupton[a,*], Robin S Langley[a]

[a]*Department of Engineering, University of Cambridge, Trumpington St, Cambridge, CB2 1PZ, UK*

## Abstract

Approximate linearised models can be important for preliminary design of floating wind turbines, but their value depends on how well they approximate the real-world non-linear behaviour. This paper focuses on the non-linear inertial coupling between motion of the floating platform and the blade dynamics, using a simplified model to demonstrate how the inertial coupling works, and systematically studying the linearity of the dynamic blade response to different directions, amplitudes and frequencies of motion. Simplified equations of motion are derived and approximately solved analytically, showing that the blade response contains harmonics at a range of frequencies, some linear and some non-linear in the amplitude of the platform motion. Comparison to numerical simulations shows that the analytical results were qualitatively useful but inaccurate for large platform motions. Because of the multiple harmonics in the response, there are more combinations of rotor speeds and platform motions leading to large resonant blade responses and non-linear behaviour than might be expected. Overall, for realistically low rotor speeds and platform frequencies (below 20 rpm and 0.2 Hz), non-linear inertial loading due to platform motion should be negligible. The implications of this work for the use of linearised structural models and the relevance of scale model testing are discussed.

*Keywords:* floating wind turbines, wind energy, non-linearity, frequency-domain modelling, structural dynamics, resonance.

## 1. Introduction

In preliminary design, approximate linearised models are attractive because they allow a broad range of designs and conditions to be explored – but they are only useful to the extent that their conclusions apply to the real-world non-linear system. The structural dynamics of a floating wind turbine – with flexible blades, in a rotating rotor, on a moving platform – are certainly complex and non-linear in theory, but is the non-linearity important in practice?

Linearised methods have been used for modelling stall-regulated turbines [1, 2], offshore turbines [3], and initial design of foundations [4] and blades [5]. For floating turbines, they have been used to study a wide space of possible concepts [6] and to test the effect of wave energy converters on spar platforms [7].

There are many sources of non-linear behaviour in floating wind turbines, from the aerodynamic and hydrodynamic loading to the control system behaviour. The importance of some of these have been studied. Non-linear hydrodynamics have been found to be negligible under some conditions [8, 9], while other non-linearities are more significant but can be approximated, such as in the aerodynamic loads and the control system dynamics [10], and viscous drag forces

---

*Corresponding author

*Email addresses:* `rcl33@cam.ac.uk` (Richard C Lupton), `rsl21@cam.ac.uk` (Robin S Langley)
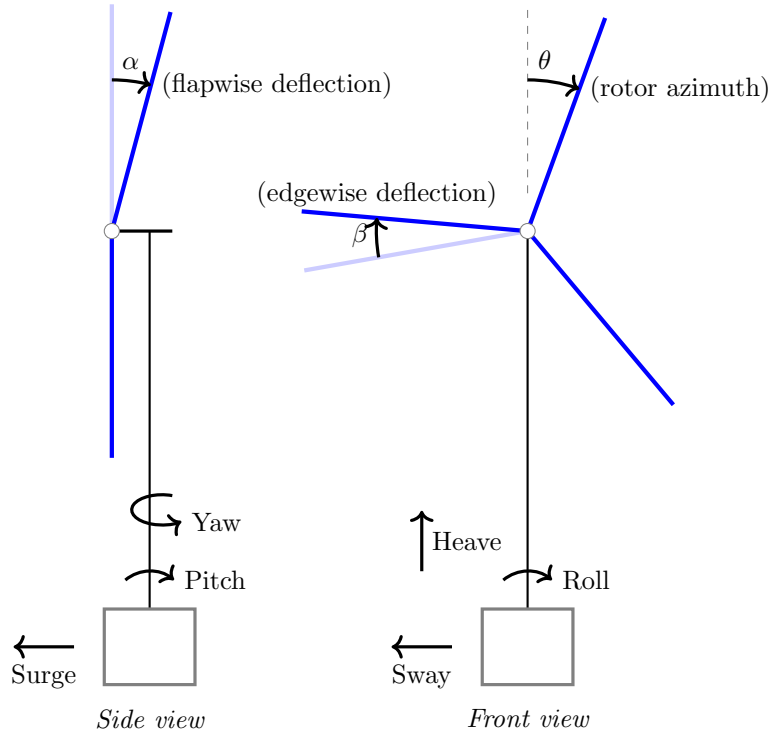
November 21, 2018

Figure 1: Simplified model of the floating wind turbine, showing types of platform motion.

on submerged structures (e.g. [11]). However, the conditions under which non-linearity in the structural dynamics is important have not been established.

In this paper we propose to focus specifically on one part of this, the non-linear inertial coupling between the motion of the platform and the blades. We use a simplified model of a floating wind turbine to systematically study the dynamic blade response to different directions, amplitudes and frequencies of prescribed platform motion. Previous preliminary results [12] are extended to cover all directions of platform motion, and identify the conditions under which non-linearity in the structural dynamics is likely to be significant. Specifically, the contributions of this paper are as follows. First, simplified equations are derived for the flapwise and edgewise blade response to each rigid-body platform motion, and approximate analytical solutions are found, which give qualitative insight into the non-linear response (Section 2). This predicts the blade responses will contain harmonics at a range of frequencies, some linear and some non-linear in the amplitude of the platform motion. Then, the response of the simplified non-linear model to each platform motion is numerically simulated over a representative range of frequencies and amplitudes, to compare against the analytical solutions, showing that they were qualitatively useful but inaccurate for large platform motions (Section 3). Summarising the combinations of rotor speeds and platform motions that lead to large resonant blade responses and non-linear behaviour shows that there are more than might be expected because of the multiple harmonics in the forcing (Section 4). Finally, the implications of this work for the use of linearised structural models and the relevance of scale model testing are discussed (Sections 5–6).

## 2. Simplified model

To isolate the effect of platform motion on the structural dynamics of the wind turbine, a simplified model is set up of a flexible turbine subject to prescribed motion in one of its 6 degrees of freedom: surge, sway and heave (translation in the $x$, $y$ and $z$ directions) and roll, pitch and
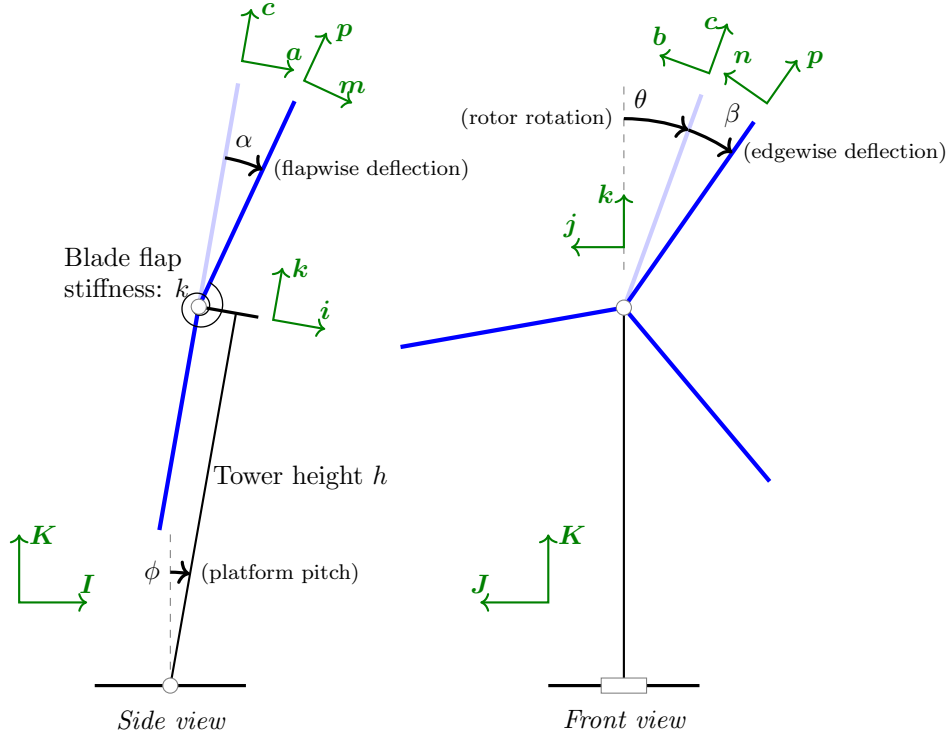
Figure 2: The simplified model of a floating wind turbine showing the flapwise blade response to platform pitching motion. The coordinates are the platform pitch angle $\phi$, the rotor azimuth angle $\theta$, the blade flapwise deflection $\alpha$ and the blade edgewise deflection $\beta$.

yaw (rotation about the $x$, $y$ and $z$ axes respectively). The flexible blades are represented by rigid beams hinged to the hub in the flapwise and edgewise directions, with hinge stiffnesses chosen to reproduce the first flapwise and edgewise natural frequencies of the blade (Figure 1). The flexibility of the tower is neglected and the rotor speed is assumed constant.

In this section the equations of motion of this simplified non-linear model are derived, before finding an approximate analytical solution for the blade response to prescribed platform motion.

### 2.1. Equations of motion – large rotations

The equations of motion are derived separately for flapwise and edgewise deflection of the blades, leading to two independent one-degree-of-freedom equations. This is an appropriate simplification if the deflections are small, but neglects the possibility of non-linear coupling between these two motions.

The particular case of platform pitch motion, shown in Figure 2, will be used as an example. In this case there are four coordinates, which are labelled in the figure. The rotor speed $\dot{\theta}(t)$ and platform pitch angle $\phi(t)$ are prescribed, leaving the blade deflection angle $\alpha(t)$ or $\beta(t)$ as the only degree of freedom. The equations of motion are derived by first finding the kinetic and potential energy functions, and then using Lagrange's equations to find the equations of motion for general platform motion, before substituting for the particular case of harmonic platform motion, with amplitude $A$ and frequency $\omega$, and constant rotor speed $\theta(t) = \Omega t$. The derivation is illustrated for the case of platform pitching motion in Appendix A, and the resulting equations for all types of motion are given in Appendix B. In total there are 12 equations of motion, for the flapwise and edgewise responses to the 6 types of platform motion (Figure 1).

3

## 2.2. Equations of motion – small rotations

It is useful to simplify the full equations of motion by assuming small blade deflections and small platform rotations. Specifically, terms are kept to first order in $\alpha$, $\beta$, and the platform motions. Again using the case of pitching motion of the platform as an example, Appendix A.5 shows the derivation of the simplified equations of motion. The result is an equation in which individual contributions can be more easily identified:

$$
\ddot{\alpha} + \left[ \underbrace{\omega_f^2}_{\substack{\text{flap} \\ \text{stiffness}}} + \underbrace{\Omega^2}_{\substack{\text{centrifugal} \\ \text{stiffness (rotor)}}} + \underbrace{\dot{\phi}^2 \left( \lambda h \cos\theta + \frac{1}{2}\cos 2\theta - \frac{1}{2} \right)}_{\substack{\text{centrifugal stiffness} \\ \text{(platform rotation)}}} - \underbrace{\lambda g \cos\theta}_{\substack{\text{gravity} \\ \text{stiffness}}} \right] \alpha
$$

$$
= \underbrace{\lambda g \phi}_{\substack{\text{out-of-plane} \\ \text{gravity load}}} + \underbrace{2\dot{\phi}\Omega \sin\theta}_{\substack{\text{Coriolis} \\ \text{force}}} - \underbrace{\ddot{\phi}\left(\lambda h + \cos\theta\right)}_{\substack{\text{platform acceleration} \\ \text{force}}} \quad (1)
$$

which after again expanding the constant rotor speed, $\theta(t) = \Omega t$, and the harmonic pitching motion, $\phi = A\sin\omega t$, becomes:

$$
\ddot{\alpha} + \left( p_f^2 - \lambda g \cos\Omega t \right)\alpha = \lambda A \left( g + h\omega^2 \right)\sin\omega t
$$

$$
+ \left( \frac{A\omega}{2} \right) \left[ (\omega + 2\Omega)\sin(\omega + \Omega)t + (\omega - 2\Omega)\sin(\omega - \Omega)t \right]
$$

$$
- \alpha \left( \frac{A\omega}{2} \right)^2 \left\{ 2\lambda h \cos\Omega t + \cos 2\Omega t - \cos 2\omega t - 1 \right.
$$

$$
+ \lambda h \left[ \cos(2\omega + \Omega)t + \cos(2\omega - \Omega)t \right]
$$

$$
\left. + \frac{1}{2}\left[ \cos 2(\omega + \Omega)t + \cos 2(\omega - \Omega)t \right] \right\} \quad (2)
$$

where all terms containing the platform amplitude $A$ have been moved to the right-hand side, and the flapwise and edgewise natural frequencies including centrifugal stiffening are written as

$$
p_f = \sqrt{\omega_f^2 + \Omega^2} \tag{3a}
$$

$$
p_e = \omega_e \tag{3b}
$$

The equation of motion is non-linear due to the interactions between the response $\alpha$ and terms related to the forcing $A\sin\omega t$. The corresponding simplified equations for the other types of platform motion are given in Appendix C.

## 2.3. Perturbation solution

The equations of motion derived above may be solved numerically, or with further approximation they may be solved analytically. In this section the perturbation method is used to find an approximate solution.

The equations of motion for small deflections, such as Equation (2) above for platform pitch and Equations (C.2)–(C.6) in Appendix C for the other platform motions, have a general form

with a force appearing on the right-hand side of the equation dependent on the current blade deflection:

$$\ddot{x}(t) + p^2 x(t) = f(t) + x(t)g(t) \tag{4}$$

where $x$ is the blade deflection response ($\alpha$ or $\beta$), $p$ is the blade's natural frequency including any centrifugal stiffening ($p_f$ or $p_e$), and $f(t)$ and $g(t)$ are the parts of the applied force which are respectively independent of and dependent on $x(t)$. The method of perturbation [13] can provide an approximate solution to a non-linear differential equation. The first step is to expand the response variable in a power series with respect to some parameter, say the amplitude of the platform motion $A$:

$$x(t) = x_0(t) + Ax_1(t) + A^2 x_2(t) + \ldots \tag{5}$$

Similarly, the applied forces can be divided into parts by the order of $A$, so that $f(t) = f_0(t) + Af_1(t) + A^2 f_2(t) + \ldots$ and equivalently for $g(t)$. Then, substituting these expansions into Equation (5) and equating powers of $A$ produces a series of linear differential equations:

$$\ddot{x}_0(t) + p^2 x_0(t) = f_0(t) \tag{6a}$$
$$\ddot{x}_1(t) + p^2 x_1(t) = f_1(t) + g_1(t)x_0(t) \tag{6b}$$
$$\ddot{x}_2(t) + p^2 x_2(t) = f_2(t) + g_2(t)x_0(t) + g_1(t)x_1(t) \tag{6c}$$
$$\ddot{x}_3(t) + p^2 x_3(t) = f_3(t) + g_3(t)x_0(t) + g_2(t)x_1(t) + g_1(t)x_2(t) \tag{6d}$$
$$\vdots$$

In this way the original non-linear equation has been transformed into a series of linear differential equations; these can be solved in turn to produce successive approximations to the full non-linear response. In theory, for the power series expansion (5) to converge, the perturbation parameter $A$ must be small. In practice useful qualitative results may be obtained even with larger values of $A$ but the amplitudes of the harmonics in the perturbation solution will not be accurate.

Because the lower-order solution becomes part of the forcing term for the higher-order solutions, when the blade response consists of multiple harmonics these will cascade through the iterations of the method. New harmonics at the sum and difference frequencies of the previous harmonics appear at every step (Figure 3), and in general the blade response to platform motion at frequency $\omega$ contains many harmonics at frequencies of the form $a\omega + b\Omega$, where $a$ and $b$ are positive or negative integers.

### 2.3.1. Damping

Damping has a strong influence on the response near resonances, so it is important to include in the approximate results. Explicitly including damping in the perturbation equations, however, is unwieldy due to the need to track phase shifts and damping factors through each iteration. Instead damping is added by modifying the final equations in a similar manner to the 'correspondence principle of linear viscoelasticity' [14].

In the model, torsional springs at the root of each blade represent the first blade bending mode. If torsional viscous dampers were added in parallel with the torsional springs, the total force would be $kx + c\dot{x}$, where $k$ is the stiffness and $c$ is the damping. Under harmonic motion, $x = Xe^{i\omega t}$, the force is $(k + ci\omega)Xe^{i\omega t}$, which is equivalent to a spring of complex stiffness $k(1 + i2\eta\omega/\omega_n)$, where $\eta$ is the damping coefficient and $\omega_n$ is the natural frequency $\sqrt{k/m}$. Therefore, to account for viscous damping, it is sufficient to replace every occurrence of the undamped natural frequency $\omega_n^2$ with

$$\omega_n^2 + i2\eta\omega\omega_n = \frac{k(1 + i2\eta\omega/\omega_n)}{m}$$
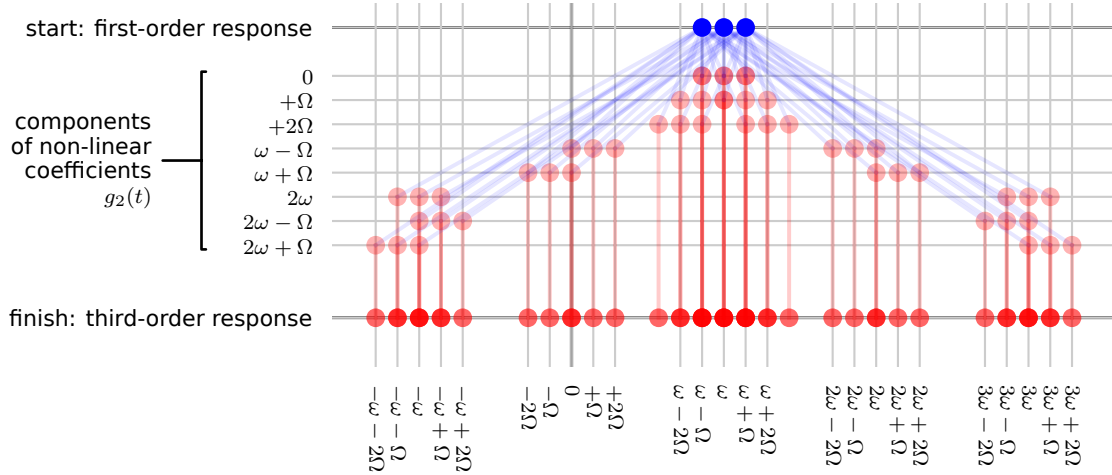
Figure 3: Development of harmonics from 1st- to 3rd-order solution for the case of the flapwise response to platform pitch. The harmonics which make up the 1st-order response are shown in the top row. When multiplied by the non-linear coefficients $g_2(t)$, new harmonics at the sum and difference frequencies are created.

The level of damping is set by the damping coefficient $\zeta$. Modelling the specific causes of damping, such as structural and aerodynamic damping effects, is outside the scope of this paper.

*2.3.2. Example: flapwise response to platform pitch motion*

The flapwise equation of motion for platform pitch motion will be used to illustrate the method of perturbation. The equation of motion (2) can be written concisely as

$$\ddot{\alpha} + p_f^2 \alpha = A f_1(t) + A^2 g_2(t)\alpha \tag{7}$$

Then substitution of a power series (5) for $\alpha$ leads to a series of linear equations like Equations (6):

$$\ddot{\alpha}_0 + p_f^2 \alpha_0 = 0 \tag{8a}$$

$$\ddot{\alpha}_1 + p_f^2 \alpha_1 = f_1(t) \tag{8b}$$

$$\ddot{\alpha}_2 + p_f^2 \alpha_2 = \alpha_0 g_2(t) \tag{8c}$$

$$\ddot{\alpha}_3 + p_f^2 \alpha_3 = \alpha_1 g_2(t) \tag{8d}$$

$$\vdots$$

These linear equations can be solved in turn to give successive approximations to the solution of the original non-linear equation.

The zeroth-order equation (8a) describes free vibration of the blade at a frequency $p_f$. Damping will, although not shown explicitly, cause this free vibration to disappear and in steady-state,

$$\alpha_0 = 0 \tag{9}$$

The first-order equation (8b), if $f_1(t)$ is written out in full, becomes

$$\ddot{\alpha}_1 + p_f^2 \alpha_1 = \lambda \left(g + h\omega^2\right) \sin \omega t$$
$$+ \frac{\omega \left(\omega + 2\Omega\right)}{2} \sin(\omega + \Omega)t$$
$$+ \frac{\omega \left(\omega - 2\Omega\right)}{2} \sin(\omega - \Omega)t$$

for which the forced vibration solution is

$$\alpha_1 = K_\omega \sin \omega t + K_+ \sin(\omega + \Omega)t + K_- \sin(\omega - \Omega)t \tag{10}$$

where

$$K_\omega = \frac{\lambda \left(g + h\omega^2\right)}{\omega_f^2 + \Omega^2 - \omega^2}$$

$$K_+ = \left(\frac{\omega}{2}\right) \frac{\omega + 2\Omega}{\omega_f^2 - \omega^2 - 2\omega\Omega}$$

$$K_- = \left(\frac{\omega}{2}\right) \frac{\omega - 2\Omega}{\omega_f^2 - \omega^2 + 2\omega\Omega}$$

This shows that the linear part of the solution consists of three harmonics: at the original forcing frequency $\omega$, and also at $\omega \pm \Omega$. This is due to the equation of motion being periodic in $\Omega$. The presence of multiple harmonics in the response of rotating blades is well known; see for example ref. [15].

Substituting the zeroth-order solution (9) into the second-order equation (8c) shows that

$$\alpha_2 = 0 \tag{11}$$

Substituting the first-order solution (10) into the third-order equation (8d) gives

$$\ddot{\alpha}_3 + p_f^2 \alpha_3 = -\left(\frac{\omega}{2}\right)^2 \left[K_\omega \sin \omega t + K_+ \sin(\omega + \Omega)t + K_- \sin(\omega - \Omega)t\right] \times$$
$$\times \left[\lambda h \cos^+(2\omega \pm \Omega)t + \frac{1}{2}\cos^+(2\omega \pm 2\Omega)t\right.$$
$$\left. + 2\lambda h \cos \Omega t + \cos 2\Omega t - \cos 2\omega t - 1\right] \tag{12}$$

where $\cos^+$ is defined in equation (C.1).

From this the solution for $\alpha_3$ can be found, but it includes so many harmonic terms at combinations of $\omega$ and $\Omega$ that it is not useful to write it out here.

Finally, the total approximate response to third order is

$$\alpha(t) = A\alpha_1(t) + A^3 \alpha_3(t) \tag{13}$$

That is, to third order, the flapwise response to platform pitch motion should include three linear harmonics at $\omega$ and $\omega \pm \Omega$, and multiple non-linear harmonics which scale with the cube of the platform motion amplitude. The approximate response determined from this procedure will be compared in the next section to the solution of the original non-linear equations.

## 3. Numerical results

The analytical results found in Section 2 give a useful qualitative understanding of non-linear components of the blade response, but depend on a series of approximations. In this

Table 1: Blade properties for numerical calculations (NREL 5 MW turbine)

| | |
|---|---|
| Blade length | 63 m |
| Flapwise natural frequency | 0.68 Hz |
| Edgewise natural frequency | 1.08 Hz |
| First moment of mass $I_1$ | 363 219 kg m |
| Second moment of mass $I_2$ | 11 753 580 kg m$^2$ |

section numerical integration of the original equations of motion (Section 2.1) is used to check the accuracy of the analytical results and present a representative range of numerical results.

For numerical calculations, the blade properties and tower height were taken from the OC3-Hywind model [16], as shown in Table 1. For simplicity, damping is set at 2 % of critical damping throughout, as actual damping varies significantly depending on the aerodynamic conditions.

Numerical simulations were run for each type of platform motion independently, for a range of amplitudes $A$, frequencies $\omega$, and rotor speeds $\Omega$. Amplitudes of platform motion up to 21 m and 19° are included. The frequency range is intended to cover the main excitation frequencies from wind and wave loading. Using the Pierson-Moskowitz or JONSWAP spectra [17], most wave energy lies within the range 0.02 Hz to 0.40 Hz, while using the IEC edition 3 Kaimal wind spectrum [18], wind energy lies below 0.12 Hz. Therefore frequencies up to 0.4 Hz are considered. A range of rotor speeds from 0 rpm to 20 rpm is considered, which encompasses the operation of current large wind turbines. Note that the although largest amplitudes of motion will not occur in practice except at the lowest frequencies, for clarity of presentation the results are calculated and plotted for a grid of values which covers all combinations.

Although the main wind and wave excitation frequencies are covered, there are some other sources of loading that could fall outside this range. Second-order wave loads can excite large low-frequency resonant motions of the platform, but the frequencies are so low this is unlikely to cause significant inertial loading on the blades. Second-order effects can also cause wave loading above the wave-energy frequency band, potentially exciting resonance of tension-leg platforms at higher frequencies. Rotational sampling of turbulence [18] causes aerodynamic loads on the platform at multiples of the rotor speed, also potentially leading to higher frequencies of platform motion. However, these effects are not considered further here.

### 3.1. Numerical solution

For each type of motion, the equation was integrated using the *odeint* function of Scipy [19]. To ensure non-linear behaviours were visible, the initial conditions were slightly perturbed from the origin. The equations were integrated for several periods until initial transients had died away, and the spectra then calculated from the remaining part of the simulation.

For example, Figure 4 shows a spectrum of the flapwise blade response for one particular set of conditions, and also the contour plot formed by combining response spectra for many frequencies of platform motion. Clearly the response contains many regularly-spaced harmonics, consistent with the prediction of the perturbation analysis of harmonics with frequencies of the form $a\omega + b\Omega$: there are sets of parallel lines, corresponding to different values of $b$, and there are multiple sets with different slopes, corresponding to different values of $a$. However, Figure 4 uses a logarithmic scale to show the structure of the response: although many harmonics are present, most of them are very small.

The derivation of the equations of motion and their numerical solution was verified by comparison to simulations using a multi-body dynamics code *mbwind* [20] and, in a few cases, the commercial wind turbine code Bladed [21]. More details are given in ref. [22].
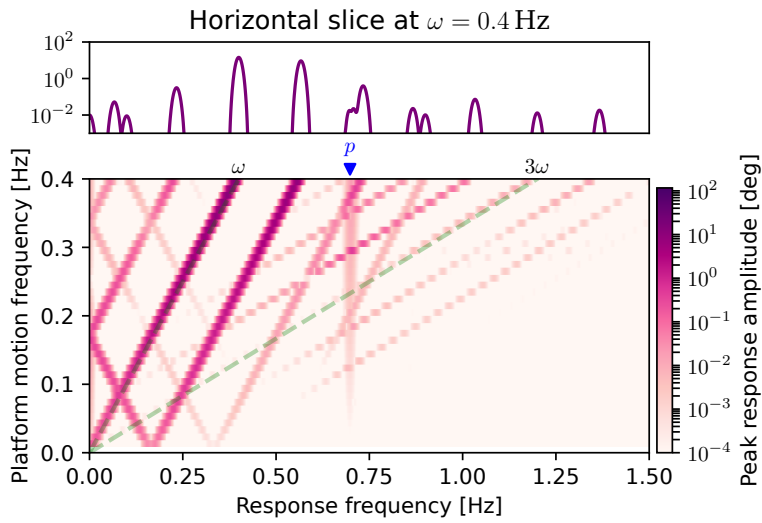
Figure 4: Simulation results showing the many harmonics present in the flapwise blade response to platform pitching motion of $\pm 11°$. The rotor speed $\Omega$ is 10 rpm. $p$ indicates the blade natural frequency. The lines labelled $\omega$ and $3\omega$ show harmonics with frequencies equal to the platform motion frequency and at $3\times$ the platform motion frequency respectively.
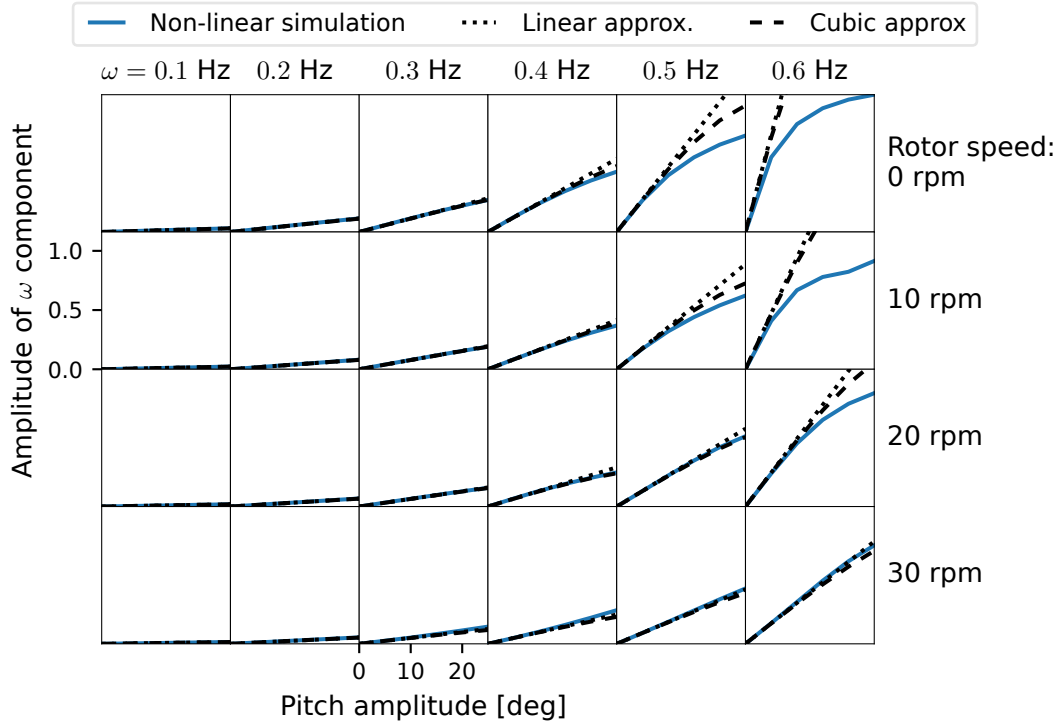


Figure 5: First- and third-order perturbation results for the $\omega$ component of the flapwise response to platform pitch motion, compared to non-linear simulation results.
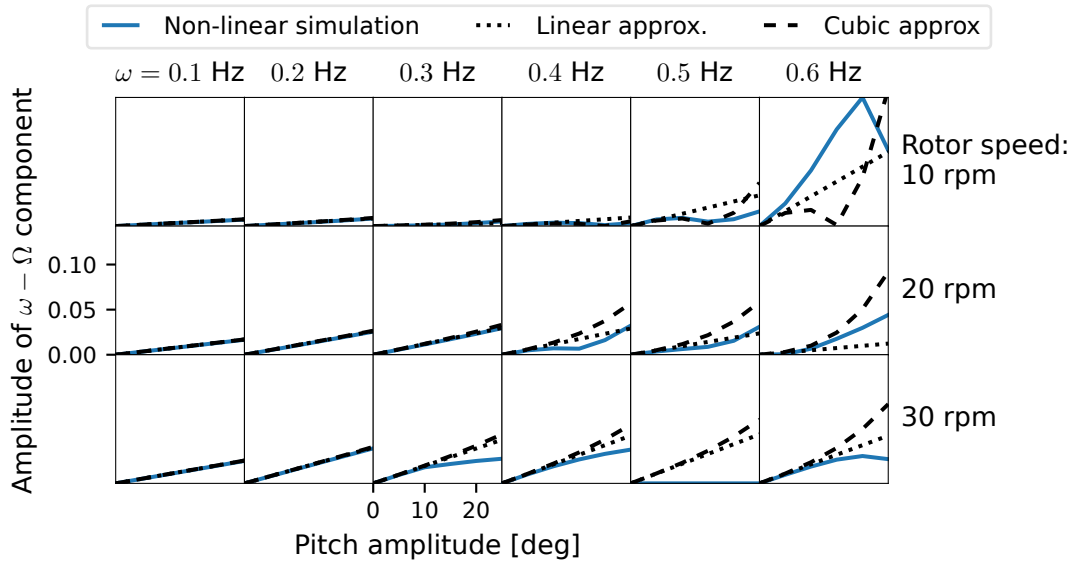
Figure 6: First- and third-order perturbation results for the $\omega - \Omega$ component of the flapwise response to platform pitch motion, compared to non-linear simulation results.
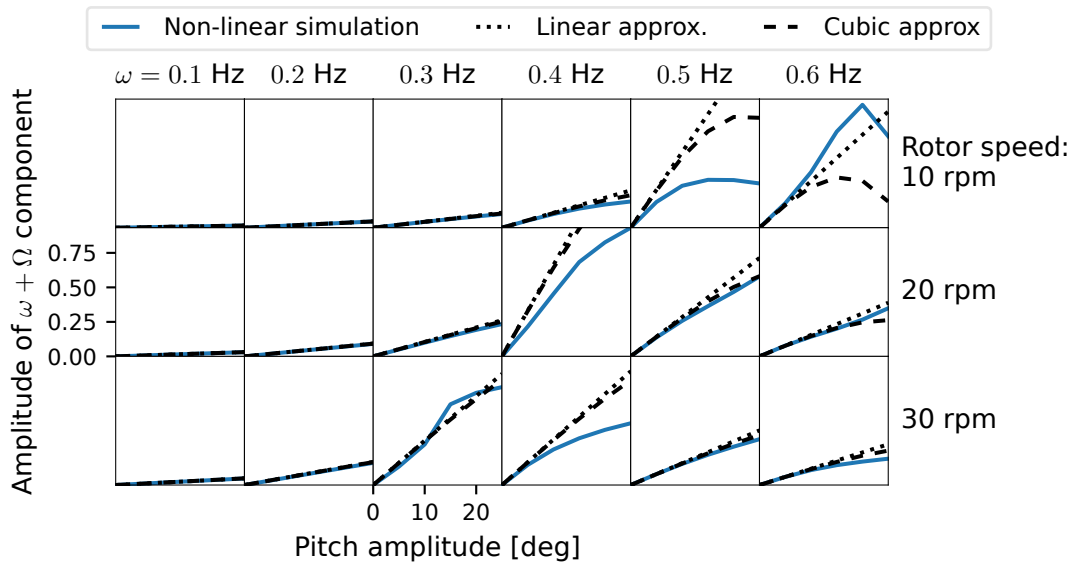


Figure 7: First- and third-order perturbation results for the $\omega + \Omega$ component of the flapwise response to platform pitch motion, compared to non-linear simulation results.
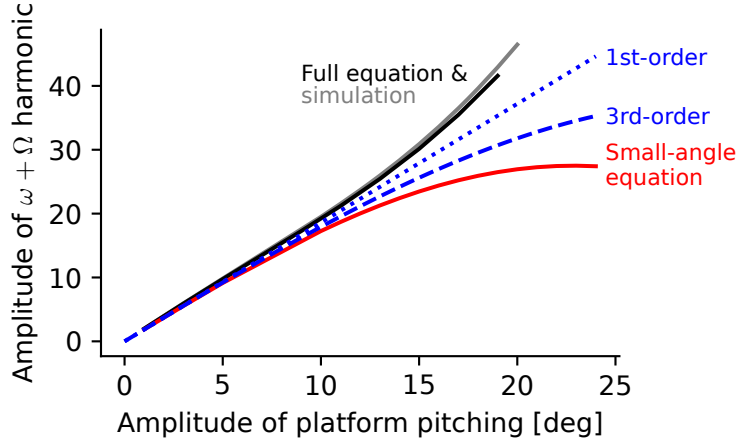
Figure 8: Comparison of small-angle approximate equation, full equation and perturbation results. Part of the error in the perturbation results is due to being based on the small-angle approximate equation of motion, which unsurprisingly does not represent the correct behaviour for large amplitudes. The results shown are the amplitude of the $\omega + \Omega$ harmonic when $\omega = 0.58\,\text{Hz}$ and $\Omega = 15\,\text{rpm}$.

### 3.2. Comparison of perturbation and numerical results

Figures 5–7 show a selection of results from the perturbation analysis (Equation 13) for various values of the rotor speed $\Omega$ and platform pitching frequency $\omega$. The three figures show the amplitude of three harmonics in the response, at $\omega$, $\omega-\Omega$ and $\omega+\Omega$. The analysis was carried out to third order in the platform motion amplitude, so both first- and third-order estimates of the response are shown. The non-linear results are also shown for comparison.

For small amplitudes, all the results agree, as expected. For larger amplitudes, generally the non-linear results increase less quickly than the linear approximation. In some cases the third-order approximation shows the same behaviour, but in others it appears to be worse than the first-order approximation.

Part of the difference between the non-linear and the perturbation results is due to the use of the approximate small-angle equations of motion, as well as the perturbation approximation itself. This is illustrated in Figure 8.

Generally, although the perturbation analysis can give an interesting insight into the blade dynamics, it is not suitable for describing the blade response for large-amplitude motion of the platform. The rest of this section focuses on the numerical results only.

### 3.3. Structure of harmonics in response to different platform motions

Figures 9–15 present results for both the flapwise and edgewise responses to all types of platform motion. In each case the rotor speed is 5 rpm, which is 0.083 Hz. This determines the horizontal spacing of the harmonics in the figures; the value is arbitrarily chosen to give a clear result. The plots show transfer functions from platform motion amplitude to blade response, and each plot shows both a large- and a small-amplitude case, giving a simple indication of non-linearity. The natural frequency of the blade is marked by an arrow at the edge of each plot. Note that unlike Figure 4, the amplitudes are shown on a linear scale.

The flapwise responses (Figures 9–11) show that surge motion causes a blade response at frequency $f = \omega$, the frequency of the platform motion, while yaw motion causes a blade response at $\omega \pm \Omega$. The response to pitch motion contains harmonics at all of these frequencies, which is expected since from the point of view of the rotor centre, pitch is a combined rotation (like yaw) and translation (like surge) motion. By comparing the small- and large-amplitude subplots, it can be seen that these flapwise responses are linear in the amplitude of platform motion.
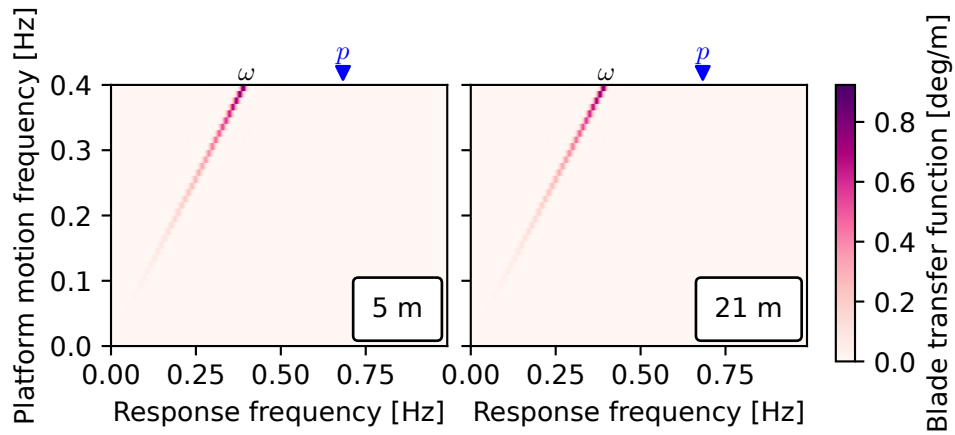
11

Figure 9: Flapwise response to platform surge motion. The response occurs purely at the forcing frequency $\omega$, and is linear. $p$ indicates the natural frequency.



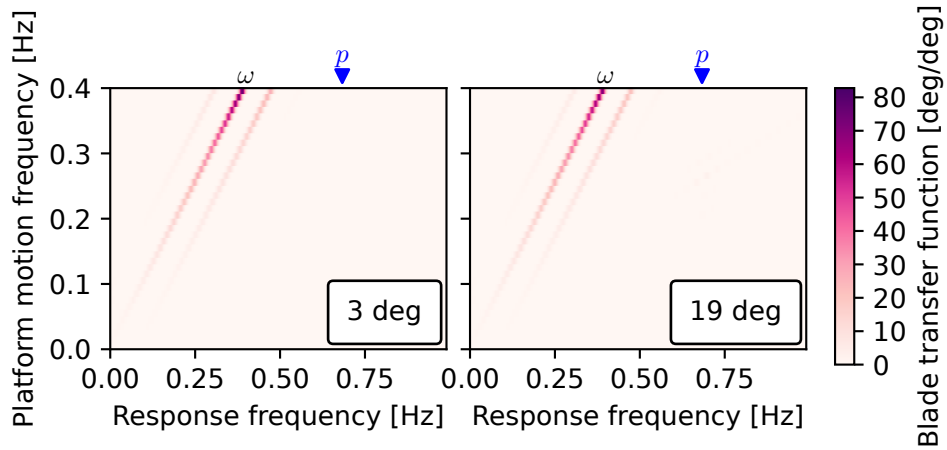Figure 10: Flapwise response to platform pitch motion. There is some response at $\omega \pm \Omega$, but most at the forcing frequency $\omega$. All harmonics are linear.
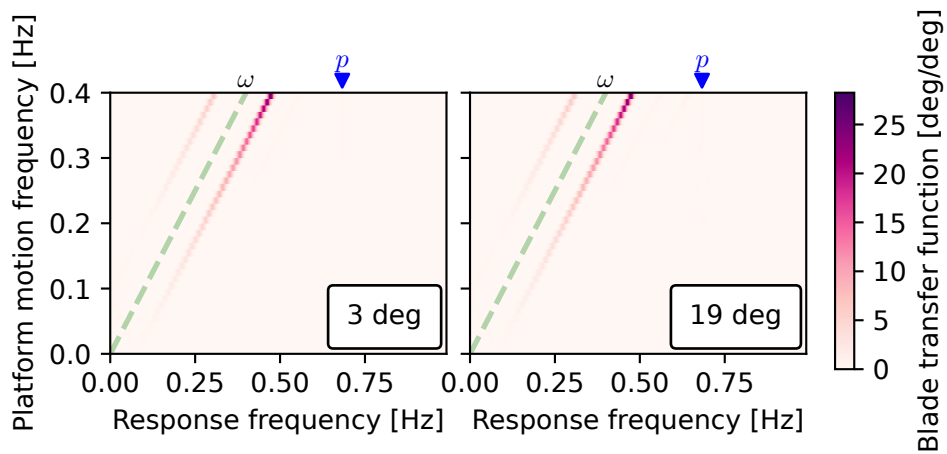


Figure 11: Flapwise response to platform yaw motion. There is no response at the forcing frequency $\omega$ (shown by the dashed line), only at $\omega \pm \Omega$. Both harmonics are linear.
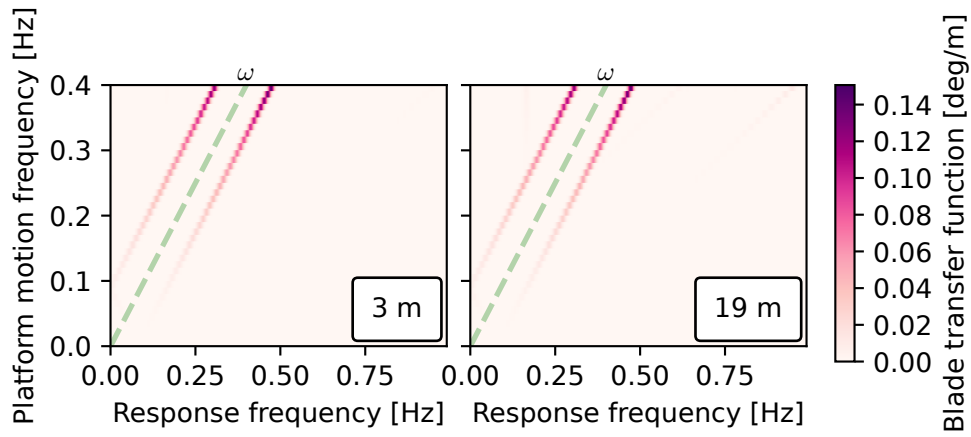
Figure 12: Edgewise response to platform heave motion. There is no response at the forcing frequency $\omega$ (shown by the dashed line), only at $\omega \pm \Omega$. Both harmonics are linear.
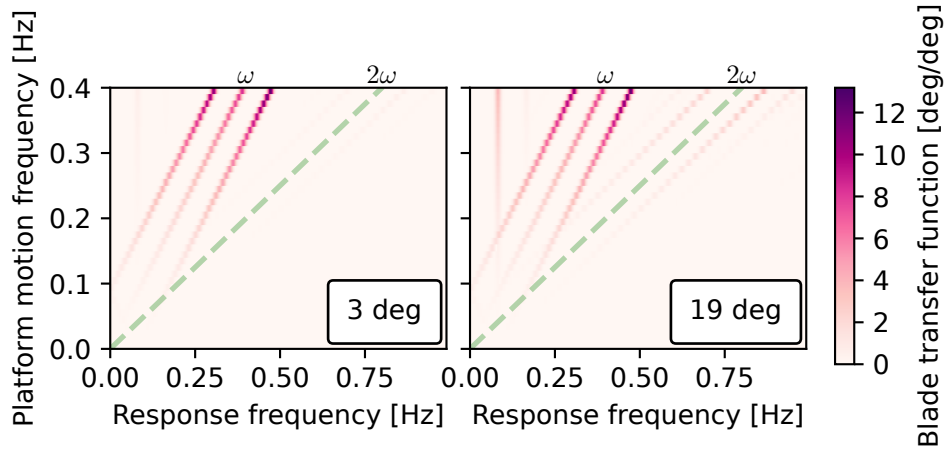


Figure 13: Edgewise response to platform roll motion. There is a linear response at $\omega$ and $\omega \pm \Omega$. Additional non-linear responses at $\Omega$ and $2\omega \pm \Omega$ are visible for larger amplitudes (on either side of the dashed line at $2\omega$).
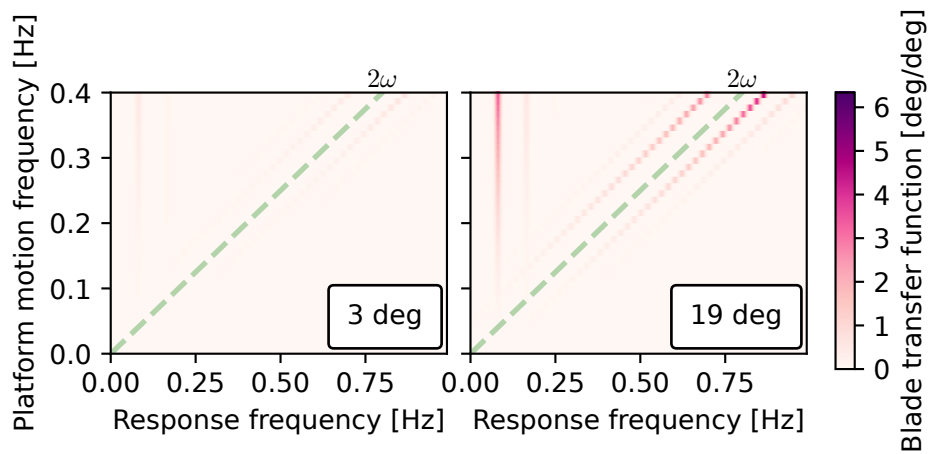


Figure 14: Edgewise response to platform pitch motion. The response is entirely non-linear, mostly at $2\omega \pm \Omega$ and $\Omega$ but also $2\omega \pm 2\Omega$ and $2\Omega$. The dashed guideline shows where the $2\omega$ harmonic would be.
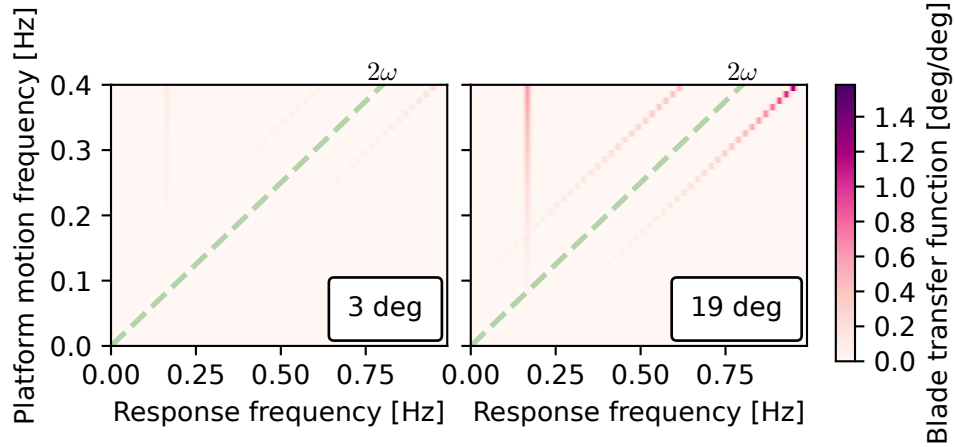
Figure 15: Edgewise response to platform yaw motion. The response is entirely non-linear, at $2\omega \pm 2\Omega$ and $2\Omega$. The dashed guideline shows where the $2\omega$ harmonic would be.

Platform heave and roll motions both cause linear edgewise blade responses (Figures 12 & 13). Heave motion causes a response at $\omega \pm \Omega$, while roll motion causes a response at both $\omega \pm \Omega$ and $\omega$. Although the two linear harmonics continue to dominate the response to heave motion even at the larger amplitudes, non-linear responses to roll motion are visible on the right of Figure 13: these appear at $\Omega$ and at $2\omega \pm \Omega$. The response to sway motion (not shown) is identical to heave, since both are a translational motion in the plane of the rotor. The responses would of course differ in a more complete model which accounted for tower flexibility.

The edgewise responses to platform pitch and yaw are purely non-linear (Figures 14 & 15), because the only inertial loading on the blades in these cases is the centrifugal force due to the rotation of the platform in pitch or yaw (as opposed to the centrifugal force due to the rotor rotation), which is proportional to the squared amplitude of the motion. Yaw motion causes responses at $2\Omega$ and $2\omega \pm 2\Omega$; these frequencies are also present in the response to pitch motion, along with larger harmonics at $\Omega$ and $2\omega \pm \Omega$.

Some types of platform motion produce no flapwise or edgewise response: surge motion produces no edgewise response, and roll and heave motion produce no flapwise responses. Although if these platform motions are superimposed on a nonzero mean pitch angle then it is possible to excite a blade response, these responses are not shown here.

In summary, the blade response contains harmonics at various frequencies. Table 2 shows the most important harmonics present in the response to each type of motion.

## 4. Conditions leading to resonance and non-linearity

The results presented in Section 3 give a detailed picture of the variety of linear and non-linear harmonics generated in the blade response to different platform motions, but it is difficult to see the bigger picture of when these are important. The presence of these harmonics has two effects: (1) with multiple harmonics, there are more conditions which can excite large resonant responses; and (2) with non-linear harmonics, the overall response is non-linear to some extent. The results from Section 3 are now summarised to show these effects.

### 4.1. Conditions leading to large blade responses

The resonant behaviour seen in the surge response in Figure 9 is unsurprising: the largest response happens when the platform motion forcing frequency approaches the blade natural frequency $\omega_f = 0.68$ Hz. What might be more surprising are the responses to other motions, when

14

Table 2: Summary of the harmonic content of the main responses. ● Linear, ○ Non-linear

| Motion | Response | $0 + \ldots$ | | $\omega + \ldots$ | | | $2\omega + \ldots$ | | | | |
|---|---|---|---|---|---|---|---|---|---|---|---|
| | | $\Omega$ | $2\Omega$ | $-\Omega$ | $0$ | $\Omega$ | $-2\Omega$ | $-\Omega$ | $0$ | $+\Omega$ | $+2\Omega$ |
| Surge | flapwise | | | | ● | | | | | | |
| Pitch | flapwise | | | ● | ● | ● | | | | | |
| Yaw | flapwise | | | ● | | ● | | | | | |
| Sway | edgewise | | | ● | | ● | | | | | |
| Heave | edgewise | | | ● | | ● | | | | | |
| Roll | edgewise | ○ | | ● | ● | ● | | ○ | | ○ | |
| Pitch | edgewise | ○ | ○ | | | | ○ | ○ | | ○ | ○ |
| Yaw | edgewise | | ○ | | | | ○ | | | | ○ |

certain combinations of platform frequency and rotor speed can excite resonance as additional harmonics coincide with the blade natural frequency.

Figure 16 shows the total blade response variance plotted against the platform motion frequency $\omega$ and the rotor speed $\Omega$. Resonances are expected around the lines $\omega = (p - b\Omega)/a$, where $a$ and $b$ are integers defining the harmonics that appear for each type of motion (Table 2) and $p$ is the natural frequency of the blade, including centrifugal stiffening for flapwise motion.

Of the flapwise responses (Figure 16 a-c), surge motion causes the simplest response. Since the only forcing is at the platform frequency $\omega$ (see also Figure 9 above), the response is simply increasing towards the blade natural frequency, located off the top of the plots. For yaw motion, the forcing is at $\omega \pm \Omega$ (Figure 11). Therefore for the same platform frequency and rotor speed, the forcing frequency due to yaw motion is higher than the forcing frequency due to surge motion, and resonance is reached in the top-right corner of Figure 16c. Pitching motion is effectively a combination of surging and yawing motions, which is reflected in the results for pitching motion in Figure 16b.

The edgewise natural frequency of the blade is higher than the flapwise frequency, so the blade is further from resonance and the edgewise responses in Figure 16(d-g) are smaller than the flapwise responses in Figure 16(a-c). Additional resonances are visible, excited by higher harmonics in the forcing: for example, at $2\omega + \Omega$ and $2\omega + 2\Omega$, as marked on the plots. These smaller resonances are the only features visible in the edgewise responses to pitch and yaw motion (Figure 16 f-g). The responses to heave and roll motion (Figure 16 d-e) are larger overall due to forcing around $\omega$. As before, the results for sway are the same as for heave and are not shown.

In summary, a general increase in response variance with increasing platform frequency $\omega$ is observed, as the forcing frequencies approach the blade natural frequencies. For the present reference turbine blade, the frequency of platform motion is always below the natural frequency of the blade, but there may be a risk that in future more flexible blades would lead to a greater response at lower frequencies. In addition, there are particular combinations of $\omega$ and $\Omega$ which lead to additional resonances (Table 3). These are due to non-linear harmonics in the inertial forcing coinciding with the blade natural frequency.

### 4.2. Linearity of blade response

The level of non-linearity in the blade response to platform motion is important for modelling the whole floating wind turbine system in the frequency domain. The results of Section 3 show that some components of the response are linear, and some non-linear, so the overall linearity of the blade response varies as the balance of different harmonic components shifts. Here overall
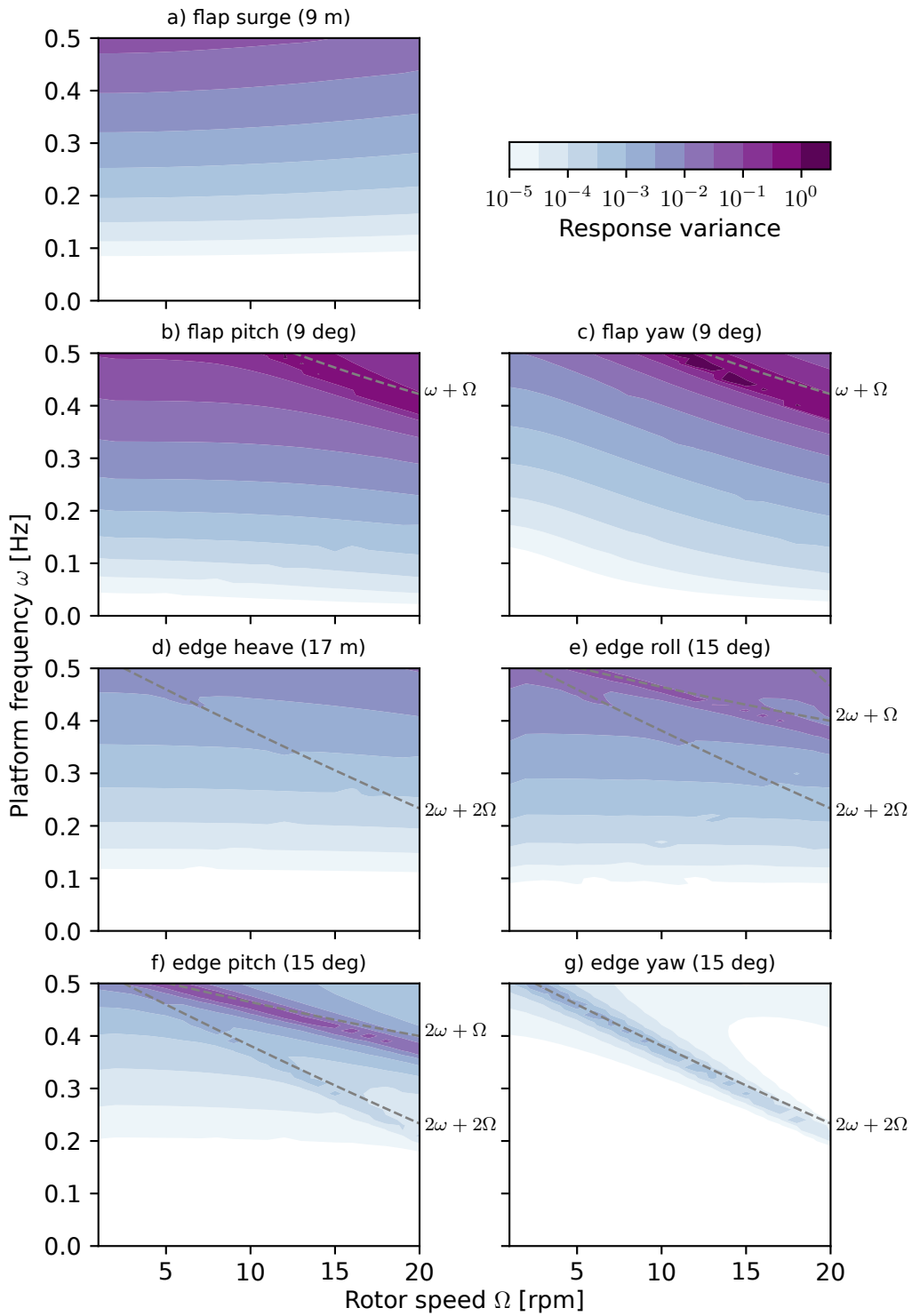
Figure 16: Blade response variance due to different platform motions.

Table 3: Local resonances (up to 0.4 Hz).

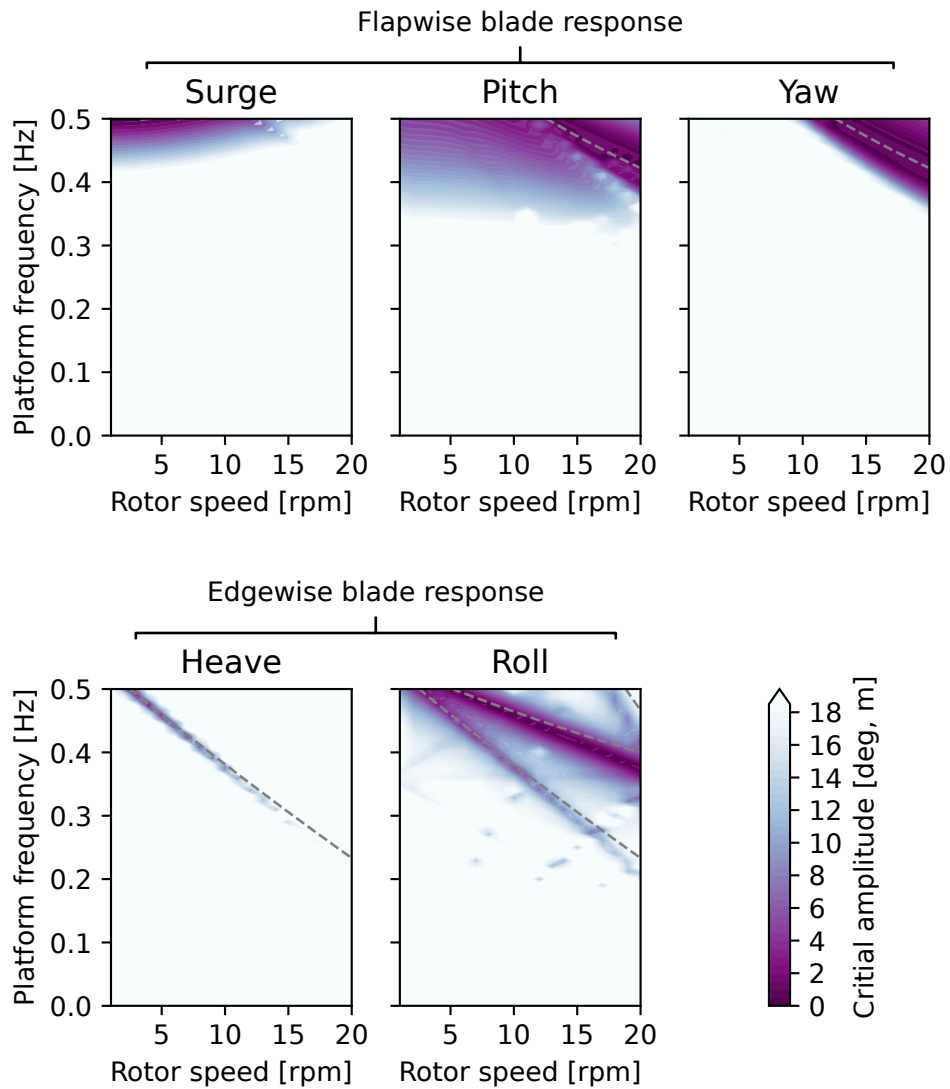| Motion | Response | $2\omega+\Omega$ | $2\omega+2\Omega$ |
|--------|----------|:----------------:|:-----------------:|
| Sway   | edgewise |                  | ● |
| Heave  | edgewise |                  | ● |
| Roll   | edgewise | ●                | ● |
| Pitch  | edgewise | ●                | ● |
| Yaw    | edgewise |                  | ● |

Figure 17: Critical motion amplitude for non-linearity to exceed 5 %.

'non-linearity' is measured as

$$\text{non-linearity}(A) = \frac{\sigma(A)/A}{\sigma(A_0)/A_0} - 1 \qquad (14)$$

where $A$ is the amplitude of the platform motion, $\sigma(A)$ is the blade response standard deviation at a given amplitude, and $A_0$ is a small reference amplitude. The non-linearity is summarised by calculating the 'critical motion amplitude', the smallest amplitude for which the non-linearity (14) exceeds a certain value.

Figure 17 plots the critical motion amplitude against platform motion frequency and rotor speed, for the flapwise response to surge, pitch and yaw, and the edgewise response to heave and roll. In the majority of conditions the pale colour of the plots indicates that even the largest amplitudes of platform motion considered were not enough to cause significant non-linear behaviour. In particular, this applies throughout the area where $\omega < 0.2\,\text{Hz}$ and $\Omega < 20\,\text{rpm}$.

There are specific combinations of platform frequency and rotor speed which lead to non-linear behaviour at moderate or even small amplitudes. These are particularly noticeable in the edgewise responses to heave (& sway) and roll motion. Note however that as the non-linearity is defined as the relative change in the transfer function, an area with high non-linearity may be irrelevant if the response there is small.

In the flapwise response to surge and pitch motion, increased non-linearity is visible at the top of the plots, for higher $\omega$. This is due to linear parts of the inertial loads exciting resonance of the hinged blade and leading to large deflections. It is the large deflections which cause the non-linear response here, and so this shows a limitation of the simplified model rather than an exact result.

The edgewise response to pitch and yaw motion are not included in Figure 17 since these responses are purely non-linear. However, they are both much smaller in magnitude than the other responses.

## 5. Implications for linearised analysis of structural dynamics

There are two issues with modelling this inertial coupling within a linearised analysis: the presence of multiple harmonics and non-linearity in the response.

The presence of multiple harmonics in the response of a rotating blade is well known, and is typically addressed by applying a Multi-Blade Coordinate (MBC) or Coleman transformation [15], in which the blade deflections are transformed into a non-rotating frame of reference. For example, the flapwise deflection of blade $k$ is expressed as

$$\alpha_k = a_0 + a_1 \cos \psi_k + b_1 \sin \psi_k \qquad (15)$$

where for a three-bladed rotor $\psi_k = \Omega t + 2\pi(k-1)/3$, and $a_0$, $a_1$ and $b_1$ are the 'multi-blade coordinates'. In this case $a_0$ represents the average flapwise deflection across all three blades, while $a_1$ and $b_1$ represent modes with a horizontal and vertical axis respectively. If the rotor is isotropic, then components of the blade response related to the rotor speed are removed: if the flapwise blade response $\alpha_k$ contains harmonics at $\omega$, $\omega - \Omega$ and $\omega + \Omega$, then the transformed coordinates $a_0$, $a_1$ and $b_1$ contain only one harmonic, at $\omega$. If the rotor is not perfectly isotropic, the MBC transformation will reduce but not eliminate the additional harmonics in the response, and the remaining periodicity is often simply neglected, or Floquet analysis can be used [23, 24].

The results in Figure 17 show that there is a large range of realistic conditions (rotor speeds below 20 rpm and platform motion frequencies below 0.2 Hz) where non-linearity in the blade response is negligible. While the exact numbers depend on the geometry of the NREL 5MW turbine used in the numerical calculations, the conclusions should apply to any similarly-scaled floating wind turbine. Because the platform motions studied are prescribed across a grid of

18

amplitudes and frequencies, rather than calculated from input wave and wind spectra, the results are not tied to the specific spar-buoy floating platform used by the NREL turbine.

On the other hand, wind turbine scales and rotor speeds may change in the future. These results show that with higher rotor speeds or more flexible blades the potential exists for multiple resonant conditions and non-linear responses.

## 6. Implications for blade dynamics at model scale

Model-scale testing is commonly used in the design of offshore structures. Although the complexity of floating wind turbines makes model testing difficult, a few tests have been performed [25, 26, 27]. Compromises are usually involved because different effects scale differently: for example, to model the wave loads correctly, the Froude number should be held constant between model and prototype scale, while to model the aerodynamic loads correctly, the Reynolds number should be held constant. Both cannot be achieved simultaneously with a geometrically-similar model, while also keeping the wind and wave forces in proportion [28].

Tests to date have focused on the dynamics of the floating platform, rather than the blades, so the models used have had rigid blades. However, the results in this paper shed some light on how dynamic effects might be observed in model-scale tests.

Dimensional analysis of the simplified blade model introduced in Section 2 shows that the non-dimensional blade response depends on six non-dimensional numbers [22]:

$$\left.\begin{array}{c}\alpha\\\beta\end{array}\right\} = F\left(\frac{g}{L_0\omega^2}, \frac{I_1}{\sqrt{mI_2}}, \frac{h}{L_0}, \frac{\Omega}{\omega}, \frac{\omega_n}{\omega}, \bar{A}\right) \tag{16}$$

where $\omega_n = \sqrt{k/I_2}$, the mass scale is $M_0 = m$, the blade mass, the time scale is $T_0 = 1/\omega$, and the length scale is $L_0 = \sqrt{I_2/m}$. The non-dimensional motion amplitude is $\bar{A} = A/L_0$ for translational motion, and just the amplitude $\bar{A} = A$ for rotational motion. Since the response depends only on these non-dimensional groups, as long as they are held constant between the prototype and model scales then the blade dynamics should be modelled correctly.

Martin et al. [28] suggest that scaled models should match the wave Froude number, the wind Froude number and the turbine Tip Speed Ratio TSR $= \Omega R/U$. For a scaling factor $\lambda$, this leads to the rotor speed scaling as $\lambda^{-1/2}$. This would be consistent with scaled modelling of the blade dynamics, which requires the rotor speed $\Omega$ to scale in proportion to the platform motion frequency $\omega$ (Equation 16).

The blade natural frequency should also scale in proportion to the rotor speed and platform motion frequency, but this may be difficult to achieve as the model blades must be very light; for example the blades of the 1/50 scale NREL 5MW turbine used by Martin et al. [28] are 1.23 m long but weigh only 140 g. In practice, model tests have used stiff blades [27] and the blade dynamics have not been considered. This means the ratio $\omega_n/\omega$ is too high. In Figure 16, the response will be towards the bottom of the plot, and non-linear parts of the response will be underestimated.

The mass distribution of the blades should be scaled to match the groups involving the first and second moments of mass in Equation (16). This would be achieved through geometric scaling and matching densities, but the scale blades are likely to have different construction. For example the aerodynamic profiles of the blade may be redesigned to deal with the lower Reynolds numbers experienced at model scale [28].

## 7. Conclusions

In this paper the dynamic response of a flexible wind turbine blade to prescribed motion of a floating platform has been systematically evaluated, for a broad range of frequencies, amplitudes and rotor speeds. The response contains many linear and non-linear harmonics, with the

potential to cause non-linearity and excite blade resonance from low-frequency platform motion, but these effects are negligible at sufficiently low rotor speeds and platform frequencies (below 20 rpm and 0.2 Hz). For a typical large offshore wind turbine, with a lower rotor speed and significant platform motion at lower frequencies than this, structural non-linearity due to platform motion should not be an issue. For the level of accuracy for which a linear structural model is acceptable for a fixed-bottom wind trubine, a linear model should also be acceptable for modelling the dynamics of a wind turbine on a floating platform.

This result therefore informs the modelling of floating wind turbines using approximate linearised methods, by showing that the specific non-linear effect studied here is likely to be negligible. However, this is only one of several sources of non-linearity in a floating wind turbine, all of which must be similarly understood. In other cases where it may not possible to neglect non-linear effects completely, such as in the aerodynamic loads and control system behaviour [10], linearised approximations can nonetheless prove useful provided their limits are well understood.

## Acknowledgements

## References

[1] A. Halfpenny, Dynamic Analysis of Both On and Offshore Wind Turbines in the Frequency Domain, Ph.D. thesis, University College London (1998).

[2] K. O. Merz, M. Muskulus, G. Moe, A simple frequency-domain method for stress analysis of stall-regulated wind turbines: Frequency-domain analysis of stall-regulated turbines, Wind Energy 15 (5) (2012) 773–798. doi:10.1002/we.504.

[3] T. G. van Engelen, Frequency Domain Analysis of Offshore Wind Turbines, Tech. rep., ECN (2004).

[4] P. van der Male, K. N. van Dalen, A. V. Metrikine, The effect of the nonlinear velocity and history dependencies of the aerodynamic force on the dynamic response of a rotating wind turbine blade, Journal of Sound and Vibration 383 (2016) 191–209. doi:10.1016/j.jsv.2016.07.031.

[5] F. E. Durá, F. M. Gimenez, J. S. Corretge, Fast Estimation of the Damage Equivalent Load in Blade Geometry Multidisciplinar Optimization, Journal of Solar Energy Engineering 139 (4) (2017) 041008. doi:10.1115/1.4036636.

[6] M. Hall, B. Buckham, C. Crawford, Evolving offshore wind: A genetic algorithm-based support structure optimization framework for floating wind turbines, IEEE, 2013, pp. 1–10. doi:10.1109/OCEANS-Bergen.2013.6608173.

[7] J. M. Kluger, T. P. Sapsis, A. H. Slocum, A reduced-order, statistical linearization approach for estimating nonlinear floating wind turbine response statistics, in: The 26th International Ocean and Polar Engineering Conference, International Society of Offshore and Polar Engineers, 2016.

[8] R. C. Lupton, R. S. Langley, Scaling of slow-drift motion with platform size and its importance for floating wind turbines, Renewable Energy 101 (2017) 1013–1020. doi:10.1016/j.renene.2016.09.052.

[9] M. Philippe, A. Babarit, P. Ferrant, Comparison of Time and Frequency Domain Simulations of an Offshore Floating Wind Turbine, in: ASME 2011 30th International Conference on Ocean, Offshore and Arctic Engineering, 2011, pp. 589–598. `doi:10.1115/OMAE2011-49722`.

[10] R. C. Lupton, R. S. Langley, Improved linearised models of wind turbine aerodynamics and control system dynamics using harmonic linearisation, Renewable Energy accepted.

[11] C. O. Housseine, C. Monroy, G. de Hauteclocque, Stochastic Linearization of the Morison Equation Applied to an Offshore Wind Turbine, ASME 2015 34th International Conference on Ocean, Offshore and Arctic Engineering (2015) V009T09A040 `doi:10.1115/OMAE2015-41301`.

[12] R. C. Lupton, Characterising dynamic non-linearity in floating wind turbines, Journal of Physics: Conference Series 555 (1) (2014) 012064. `doi:10.1088/1742-6596/555/1/012064`.

[13] J. J. Stoker, Nonlinear Vibrations, Interscience Publishers Ltd, New York, 1950.

[14] D. R. Bland, The theory of linear viscoelasticity, Pergamon Press, 1960.

[15] M. H. Hansen, Aeroelastic Instability Problems for Wind Turbines, Wind Energy 10 (6) (2007) 551–577. `doi:10.1002/we`.

[16] J. Jonkman, S. Butterfield, W. Musial, G. Scott, Definition of a 5-MW Reference Wind Turbine for Offshore System Development, Tech. Rep. February, National Renewable Energy Laboratory, Golden, USA (2009).

[17] S. K. Chakrabarti, Handbook of offshore engineering, Elsevier, 2005.

[18] T. Burton, D. Sharpe, N. Jenkins, E. Bossanyi, Wind Energy Handbook, John Wiley & Sons, 2011.

[19] E. Jones, T. Oliphant, P. Peterson, others, SciPy: Open source scientific tools for Python (2001).
URL `http://www.scipy.org/`

[20] R. C. Lupton, Mbwind v1.0 (Apr. 2018). `doi:10.5281/zenodo.1221056`.
URL `https://zenodo.org/record/1221056`

[21] Garrad Hassan, Bladed Theory Manual, Tech. rep. (2011).

[22] R. C. Lupton, Frequency-domain modelling of floating wind turbines, Ph.D. thesis, University of Cambridge (2015).
URL `https://doi.org/10.17863/CAM.14119`

[23] K. Stol, M. Balas, G. Bir, Floquet Modal Analysis of a Teetered-Rotor Wind Turbine, Journal of Solar Energy Engineering 124 (4) (2002) 364–371. `doi:10.1115/1.1504846`.
URL `http://link.aip.org/link/JSEEDO/v124/i4/p364/s1&Agg=doi`

[24] P. F. Skjoldan, M. H. Hansen, Implicit Floquet analysis of wind turbines using tangent matrices of a non-linear aeroelastic code, Wind Energy.

[25] D. G. Roddier, C. A. Cermelli, A. Aubault, A. Weinstein, WindFloat: A floating foundation for offshore wind turbines, Journal of Renewable and Sustainable Energy 2 (3) (2010) 033104. `doi:10.1063/1.3435339`.

[26] F. G. Nielsen, T. D. Hanson, B. r. Skaare, Integrated Dynamic Analysis of Floating Offshore Wind Turbines, in: Proceedings of the 25th International Conference on Offshore Mechanics and Arctic Engineering, Hydro Oil & Energy, Hamburg, Germany, 2006. doi:10.1115/OMAE2006-92291.

[27] A. J. Goupee, K. F. Lambrakos, R. W. Kimball, B. Koo, H. J. Dagher, Experimental comparison of three floating wind turbine concepts, in: Proceedings of the 31st International Conference on Offshore Mechanics and Arctic Engineering, ASME, Rio de Janeiro, Brazil, 2012.

[28] H. R. Martin, R. W. Kimball, A. M. Viselli, A. J. Goupee, Methodology for Wind/Wave Basin Testing of Floating Offshore Wind Turbines, Journal of Offshore Mechanics and Arctic Engineering 136 (2) (2014) 021902. doi:10.1115/1.4025030.

[29] SymPy Development Team, SymPy: Python library for symbolic mathematics (2012). URL http://www.sympy.org

## Appendix A. Kinematics for platform pitching motion

Although in practice the equations of motion were derived for general platform motion using a computer algebra system, the resulting equations are rather long and difficult to understand. Rather than presenting the general equations, here the simpler case of platform pitching motion is used to illustrate the procedure.

### Appendix A.1. Coordinate systems

The model, shown in Figure 2, is described by several coordinate systems, which in this case are related as follows:

1. A fixed coordinate system $IJK$.

2. Rotation of $IJK$ through an angle $\phi$ about the $J$ axis gives the platform coordinate system $ijk$.

3. Rotation of $ijk$ through an angle $\theta$ about the $i$ axis gives the blade root coordinate system $abc$. The rotor axis is located at a height $h$.

4. For flapwise and edgewise deflections respectively:

    (a) Rotation of $abc$ through an angle $\alpha$ about the $b$ axis gives the blade-fixed coordinate system $mnp$, where $n = b$. This rotation represents the blade flexibility in the flapwise direction.

    (b) Rotation of $abc$ through an angle $\beta$ about the $a$ axis gives the blade-fixed coordinate system $mnp$, where $m = a$. This rotation represents the blade flexibility in the edgewise direction.

The turbine unit vectors and their derivatives are related to the fixed unit vectors as follows:

$$i = I \cos \phi - K \sin \phi \qquad\qquad \dot{i} = -\dot{\phi} k \qquad\qquad \text{(A.1a)}$$

$$j = J \qquad\qquad \dot{j} = 0 \qquad\qquad \text{(A.1b)}$$

$$k = K \cos \phi + I \sin \phi \qquad\qquad \dot{k} = \dot{\phi} i \qquad\qquad \text{(A.1c)}$$

The rotor unit vectors and their derivatives are related to the turbine unit vectors as follows:

$$a = i \qquad\qquad \dot{a} = -\dot{\phi} k \qquad\qquad \text{(A.2a)}$$

$$b = j \cos \theta + k \sin \theta \qquad\qquad \dot{b} = \dot{\theta} c + \dot{\phi} \sin \theta i \qquad\qquad \text{(A.2b)}$$

$$c = -j \sin \theta + k \cos \theta \qquad\qquad \dot{c} = -\dot{\theta} b + \dot{\phi} \cos \theta i \qquad\qquad \text{(A.2c)}$$

For flapwise deflections, the blade unit vectors are related to the rotor unit vectors as follows:

$$m = -c \sin \alpha + a \cos \alpha \qquad\qquad \dot{m} = -\dot{\alpha} p - \dot{\phi} \cos \alpha k \qquad\qquad \text{(A.3a)}$$
$$+ \sin \alpha \left( \dot{\theta} b - \dot{\phi} \cos \theta i \right)$$

$$n = b \qquad\qquad \dot{n} = \dot{\theta} c + \dot{\phi} \sin \theta i \qquad\qquad \text{(A.3b)}$$

$$p = c \cos \alpha + a \sin \alpha \qquad\qquad \dot{p} = \dot{\alpha} m - \dot{\phi} \sin \alpha k \qquad\qquad \text{(A.3c)}$$
$$- \cos \alpha \left( \dot{\theta} b - \dot{\phi} \cos \theta i \right)$$

while for edgewise deflections,

$$\boldsymbol{m} = \boldsymbol{a} \qquad\qquad \dot{\boldsymbol{m}} = -\dot{\phi}\boldsymbol{k} \tag{A.4a}$$

$$\boldsymbol{n} = \boldsymbol{b}\cos\beta + \boldsymbol{c}\sin\beta \qquad\qquad \dot{\boldsymbol{n}} = \dot{\beta}\boldsymbol{p} + \cos\beta\left(\dot{\theta}\boldsymbol{c} + \dot{\phi}\sin\theta\boldsymbol{i}\right) \tag{A.4b}$$

$$+ \sin\beta\left(-\dot{\theta}\boldsymbol{b} + \dot{\phi}\cos\theta\boldsymbol{i}\right)$$

$$\boldsymbol{p} = \boldsymbol{c}\cos\beta - \boldsymbol{b}\sin\beta \qquad\qquad \dot{\boldsymbol{p}} = -\dot{\beta}\boldsymbol{n} + \cos\beta\left(-\dot{\theta}\boldsymbol{b} + \dot{\phi}\cos\theta\boldsymbol{i}\right) \tag{A.4c}$$

$$+ \sin\beta\left(\dot{\theta}\boldsymbol{c} + \dot{\phi}\sin\theta\boldsymbol{i}\right)$$

*Appendix A.2. Blade kinematics*

The position of an arbitrary point on the blade (at radius $r$) is

$$\boldsymbol{r} = h\boldsymbol{k} + r\boldsymbol{p} \tag{A.5}$$

By differentiating this, and using the coordinate system relationships above, the velocity is found to be

$$\dot{\boldsymbol{r}} = \dot{\phi}\left(h + r\cos\alpha\cos\theta\right)\boldsymbol{i} - r\dot{\phi}\sin\alpha\boldsymbol{k} - r\dot{\theta}\cos\alpha\boldsymbol{b} + r\dot{\alpha}\boldsymbol{m} \tag{A.6a}$$

for flapwise deflections, and

$$\dot{\boldsymbol{r}} = \dot{\phi}\left(h + r\cos\beta\cos\theta - r\sin\beta\sin\theta\right)\boldsymbol{i} - r\left(\dot{\theta} + \dot{\beta}\right)\boldsymbol{n} \tag{A.6b}$$

for edgewise deflections. To find the kinetic energy, the speed is needed. The relevant dot products to evaluate $\dot{\boldsymbol{r}} \cdot \dot{\boldsymbol{r}}$ can be found from equations (A.1)–(A.4). For flapwise deflections, the only non-zero products are

$$\boldsymbol{i} \cdot \boldsymbol{m} = \cos\alpha \qquad\qquad \boldsymbol{k} \cdot \boldsymbol{m} = -\sin\alpha\cos\theta \qquad\qquad \boldsymbol{k} \cdot \boldsymbol{b} = \sin\theta \tag{A.7}$$

while for edgewise deflections, $\boldsymbol{i} \cdot \boldsymbol{n} = 0$. The speed squared is therefore

$$\dot{\boldsymbol{r}} \cdot \dot{\boldsymbol{r}} = \left[(h + r\cos\alpha\cos\theta)^2 + (r\sin\alpha)^2\right]\dot{\phi}^2 + (r\cos\alpha)^2\dot{\theta}^2 + r^2\dot{\alpha}^2$$
$$+ 2r\dot{\alpha}\dot{\phi}\left(h\cos\alpha + r\cos\theta\right) + r^2\dot{\phi}\dot{\theta}\sin 2\alpha\sin\theta \tag{A.8a}$$

for flapwise deflections, and

$$\dot{\boldsymbol{r}} \cdot \dot{\boldsymbol{r}} = (h + r\cos\beta\cos\theta - r\sin\beta\sin\theta)^2\dot{\phi}^2 + r^2\left(\dot{\theta} + \dot{\beta}\right)^2 \tag{A.8b}$$

for edgewise deflections.

To find the potential energy, the height of an arbitrary point on the blade is also needed. From Equation (A.5),

$$H = \boldsymbol{r} \cdot \boldsymbol{K} = h\cos\phi + r\left(\cos\alpha\cos\theta\cos\phi - \sin\alpha\sin\theta\right) \tag{A.9a}$$

for flapwise deflections, and

$$H = \boldsymbol{r} \cdot \boldsymbol{K} = h\cos\phi + r\cos\phi\left(\cos\beta\cos\theta - \sin\beta\sin\theta\right) \tag{A.9b}$$

for edgewise deflections.

24

*Appendix A.3. Kinetic and potential energy*

The kinetic energy of the blade is given by

$$T = \frac{1}{2} \int (\boldsymbol{r} \cdot \boldsymbol{r}) \, \mathrm{d}m \tag{A.10}$$

Substituting the expressions for the speed at radius $r$ from Equations (A.8) gives

$$2T = \left[ Mh^2 + 2hI_1 \cos \alpha \cos \theta + I_2 \cos^2 \alpha \cos^2 \theta + I_2 \sin^2 \alpha \right] \dot{\phi}^2$$
$$+ I_2 \cos^2 \alpha \dot{\theta}^2 + I_2 \dot{\alpha}^2 + 2\dot{\alpha}\dot{\phi} \left( hI_1 \cos \alpha + I_2 \cos \theta \right) + I_2 \dot{\phi}\dot{\theta} \sin 2\alpha \sin \theta \tag{A.11a}$$

for flapwise deflections, and

$$2T = \left[ Mh^2 + 2hI_1 \left( \cos \beta \cos \theta - \sin \beta \sin \theta \right) \right.$$
$$\left. + I_2 \left( \cos \beta \cos \theta - \sin \beta \sin \theta \right)^2 \right] \dot{\phi}^2 + I_2 \left[ \dot{\theta} + \dot{\beta} \right]^2 \tag{A.11b}$$

for edgewise deflections, where $M$ is the blade's mass, and $I_1$ and $I_2$ are its first and second moments of mass, defined as

$$M = \int \mathrm{d}m \tag{A.12a}$$

$$I_1 = \int r \, \mathrm{d}m \tag{A.12b}$$

$$I_2 = \int r^2 \, \mathrm{d}m \tag{A.12c}$$

The potential energy is

$$V = \frac{1}{2} k_f \alpha^2 + Mgh \cos \phi + I_1 g \left( \cos \alpha \cos \phi \cos \theta - \sin \alpha \sin \phi \right) \tag{A.13a}$$

for flapwise deflections, and

$$V = \frac{1}{2} k_e \beta^2 + Mgh \cos \phi + I_1 g \cos \phi \left( \cos \beta \cos \theta - \sin \beta \sin \theta \right) \tag{A.13b}$$

for edgewise deflections, and the stiffness of the blade hinge is $k_f$ and $k_e$ in the flapwise and edgewise directions respectively.

*Appendix A.4. Full equation of motion*

The kinetic and potential energies lead to the equation of motion through Lagrange's equation:

$$\frac{\mathrm{d}}{\mathrm{d}t} \left[ \frac{\partial T}{\partial \dot{\alpha}} \right] - \frac{\partial T}{\partial \alpha} + \frac{\partial V}{\partial \alpha} = Q_\alpha \tag{A.14}$$

For the blade flapwise response to platform pitch motion, these terms are:

$$\frac{\partial T}{\partial \dot{\alpha}} = I_2 \dot{\alpha} + \dot{\phi} \left( I_1 h \cos \alpha + I_2 \cos \theta \right) \tag{A.15a}$$

$$\frac{\mathrm{d}}{\mathrm{d}t} \left[ \frac{\partial T}{\partial \dot{\alpha}} \right] = I_2 \ddot{\alpha} + \ddot{\phi} \left( I_1 h \cos \alpha + I_2 \cos \theta \right) - \dot{\phi} \left( I_1 h \dot{\alpha} \sin \alpha + I_2 \dot{\theta} \sin \theta \right) \tag{A.15b}$$

$$\frac{\partial T}{\partial \alpha} = \dot{\phi}^2 \left( I_2 \cos \alpha \left( 1 - \cos^2 \theta \right) - I_1 h \cos \theta \right) \sin \alpha$$
$$+ \dot{\phi} \left( I_2 \dot{\theta} \sin \theta \cos 2\alpha - I_1 h \dot{\alpha} \sin \alpha \right) - I_2 \dot{\theta}^2 \sin \alpha \cos \alpha \tag{A.15c}$$

$$\frac{\partial V}{\partial \alpha} = k\alpha - I_1 g \left( \sin \alpha \cos \phi \cos \theta + \cos \alpha \sin \phi \right) \tag{A.15d}$$

$$Q = 0 \tag{A.15e}$$

25

Substituting these into Equation (A.14) leads directly to the equation of motion. The equation of motion for the edgewise response is derived in exactly the same way, but for brevity is not written in full. All the equations of motion, assuming harmonic motion of the platform, are given in Appendix Appendix B below.

*Appendix A.5. Small-angle equation of motion*

Some simplifications can be introduced to allow for further analysis. The rotor speed is assumed constant with $\Omega = \dot{\theta}$. The flap angle will be assumed to be small, such that $\sin \alpha \approx \alpha$ and $\cos \alpha \approx 1$. This is reasonable because the flap angle is a simplified model of the blade's flexibility which is only realistic for small deflections. The potential energy (A.13) contains the terms $\sin \phi$ and $\cos \phi$, but the platform motion $\phi$ is assumed to be small, so $\sin \phi \approx \phi$ and $\cos \phi \approx 1$. Finally, a factor of $I_2$ is removed and the ratio $\lambda = I_1/I_2$ is introduced. With these simplifications, the terms in (A.15) become

$$\frac{\mathrm{d}}{\mathrm{d}t}\left[\frac{\partial T}{\partial \dot{\alpha}}\right] = \ddot{\alpha} + \ddot{\phi}\left(\lambda h + \cos \theta\right) - \dot{\phi}\left(\lambda h \dot{\alpha}\alpha + \Omega \sin \theta\right) \tag{A.16a}$$

$$\frac{\partial T}{\partial \alpha} = \left(\dot{\phi}^2\left(1 - \cos^2 \theta - \lambda h \cos \theta\right) - \lambda h \dot{\phi}\dot{\alpha} - \Omega^2\right)\alpha + \dot{\phi}\Omega \sin \theta \tag{A.16b}$$

$$\frac{\partial V}{\partial \alpha} = \omega_f^2 \alpha - \lambda g\left(\alpha \cos \theta + \phi\right) \tag{A.16c}$$

where $\omega_f^2 = k/I_2$ is the natural frequency of the blade. Substituting into Equation (A.14) shows the simplified equation of motion for the blade flap motion to be

$$\ddot{\alpha} + \left[\omega_f^2 + \Omega^2 + \dot{\phi}^2\left(\lambda h \cos \theta + \frac{1}{2}\cos 2\theta - \frac{1}{2}\right) - \lambda g \cos \theta\right]\alpha =$$
$$\lambda g \phi + 2\dot{\phi}\Omega \sin \theta - \ddot{\phi}\left(\lambda h + \cos \theta\right) \tag{A.17}$$

All the simplified equations of motion are given in Appendix Appendix C below.

## Appendix B. Full equations of motion

For the particular case of harmonic platform motion, with amplitude $A$ and frequency $\omega$, the results are presented below. In total there are 12 equations of motion, for the flapwise and edgewise responses to the 6 types of platform motion (Figure 1). The equations were derived as shown in the example given in Appendix A, but making use of the SymPy symbolic algebra package [29], and the results are listed below. $\omega_f = \sqrt{k_f/I_2}$ and $\omega_e = \sqrt{k_e/I_2}$ are the flapwise and edgewise natural frequencies respectively, and $\lambda = I_1/I_2$ is the ratio of first and second moments of mass of the blade. The rotor speed $\Omega$ is assumed constant so $\theta(t) = \Omega t$.

*Surge*
Flapwise:

$$-A\lambda\omega^2 \sin \omega t \cos \alpha + \Omega^2 \sin \alpha \cos \alpha - g\lambda \sin \alpha \cos \Omega t + \omega_f^2 \alpha + \ddot{\alpha} = 0 \tag{B.1}$$

Edgewise:

$$-g\lambda \sin \Omega t \cos \beta - g\lambda \sin \beta \cos \Omega t + \omega_e^2 \beta + \ddot{\beta} = 0 \tag{B.2}$$

*Sway*
Platform sway motion, as an in-plane translation of the rotor, is similar to heave motion and yields the same equations as given below.

*Heave*
Flapwise:

$$A\lambda\omega^2 \sin\omega t \sin\alpha \cos\Omega t \;+\; \Omega^2 \sin\alpha \cos\alpha \;-\; g\lambda \sin\alpha \cos\Omega t \;+\; \omega_f^2 \alpha \;+\; \ddot{\alpha} \;=\; 0 \quad \text{(B.3)}$$

Edgewise:

$$A\lambda\omega^2 \sin\Omega t \sin\omega t \cos\beta + A\lambda\omega^2 \sin\omega t \sin\beta \cos\Omega t$$
$$- g\lambda \sin\Omega t \cos\beta - g\lambda \sin\beta \cos\Omega t + \omega_e^2 \beta + \ddot{\beta} = 0 \quad \text{(B.4)}$$

*Roll*
Flapwise:

$$A^2 h\lambda\omega^2 \sin\alpha \cos\Omega t \cos^2\omega t + A^2\omega^2 \sin\alpha \cos^2\omega t \cos\alpha$$
$$+ 2A\Omega\omega \sin\alpha \cos\omega t \cos\alpha + Ah\lambda\omega^2 \sin\Omega t \sin\omega t \sin\alpha$$
$$+ \Omega^2 \sin\alpha \cos\alpha + g\lambda \sin(A\sin\omega t) \sin\Omega t \sin\alpha$$
$$- g\lambda \sin\alpha \cos(A\sin\omega t) \cos\Omega t + \omega_f^2 \alpha + \ddot{\alpha} = 0 \quad \text{(B.5)}$$

Edgewise:

$$A^2 h\lambda\omega^2 \sin\Omega t \cos^2\omega t \cos\beta + A^2 h\lambda\omega^2 \sin\beta \cos\Omega t \cos^2\omega t$$
$$+ Ah\lambda\omega^2 \sin\Omega t \sin\omega t \sin\beta - Ah\lambda\omega^2 \sin\omega t \cos\Omega t \cos\beta$$
$$- A\omega^2 \sin\omega t + g\lambda \sin(A\sin\omega t) \sin\Omega t \sin\beta$$
$$- g\lambda \sin(A\sin\omega t) \cos\Omega t \cos\beta - g\lambda \sin\Omega t \cos(A\sin\omega t) \cos\beta$$
$$- g\lambda \sin\beta \cos(A\sin\omega t) \cos\Omega t + \omega_e^2 \beta + \ddot{\beta} = 0 \quad \text{(B.6)}$$

*Pitch*
Flapwise:

$$A^2 h\lambda\omega^2 \sin\alpha \cos\Omega t \cos^2\omega t + A^2\omega^2 \sin\alpha \cos^2\Omega t \cos^2\omega t \cos\alpha$$
$$- A^2\omega^2 \sin\alpha \cos^2\omega t \cos\alpha - 2A\Omega\omega \sin\Omega t \cos\omega t \cos^2\alpha$$
$$- Ah\lambda\omega^2 \sin\omega t \cos\alpha - A\omega^2 \sin\omega t \cos\Omega t + \Omega^2 \sin\alpha \cos\alpha$$
$$- g\lambda \sin(A\sin\omega t) \cos\alpha - g\lambda \sin\alpha \cos(A\sin\omega t) \cos\Omega t$$
$$+ \omega_f^2 \alpha + \ddot{\alpha} = 0 \quad \text{(B.7)}$$

Edgewise:

$$A^2 h\lambda\omega^2 \sin\Omega t \cos^2\omega t \cos\beta + A^2 h\lambda\omega^2 \sin\beta \cos\Omega t \cos^2\omega t$$
$$- A^2\omega^2 \sin^2\Omega t \sin\beta \cos^2\omega t \cos\beta - A^2\omega^2 \sin\Omega t \sin^2\beta \cos\Omega t \cos^2\omega t$$
$$+ A^2\omega^2 \sin\Omega t \cos\Omega t \cos^2\omega t \cos^2\beta + A^2\omega^2 \sin\beta \cos^2\Omega t \cos^2\omega t \cos\beta$$
$$- g\lambda \sin\Omega t \cos(A\sin\omega t) \cos\beta - g\lambda \sin\beta \cos(A\sin\omega t) \cos\Omega t$$
$$+ \omega_e^2 \beta + \ddot{\beta} = 0 \quad \text{(B.8)}$$

*Yaw*
Flapwise:

$$A^2\omega^2 \sin^2\Omega t \sin\alpha \cos^2\omega t \cos\alpha - A^2\omega^2 \sin\alpha \cos^2\omega t \cos\alpha$$
$$+ 2A\Omega\omega \cos\Omega t \cos\omega t \cos^2\alpha - A\omega^2 \sin\Omega t \sin\omega t + \Omega^2 \sin\alpha \cos\alpha$$
$$- g\lambda \sin\alpha \cos\Omega t + \omega_f^2 \alpha + \ddot{\alpha} = 0 \quad \text{(B.9)}$$

27

Edgewise:

$$A^2\omega^2 \sin^2 \Omega t \sin\beta \cos^2 \omega t \cos\beta + A^2\omega^2 \sin\Omega t \sin^2\beta \cos\Omega t \cos^2\omega t$$
$$- A^2\omega^2 \sin\Omega t \cos\Omega t \cos^2\omega t \cos^2\beta - A^2\omega^2 \sin\beta \cos^2\Omega t \cos^2\omega t \cos\beta$$
$$- g\lambda \sin\Omega t \cos\beta - g\lambda \sin\beta \cos\Omega t$$
$$+ \omega_e^2\beta + \ddot\beta = 0 \quad \text{(B.10)}$$

## Appendix C. Small-angle equations of motion

Below, the equivalent simplified equations are presented for other types of platform motion. A parametric excitation term due to gravity, visible on the left-hand side of Equation (2), has been neglected since $(p_f^2/\lambda g) \gg 1$ for the blade of the reference wind turbine (the NREL 5 MW). For brevity, the notation is introduced that

$$\sin^+(A \pm B) = \sin(A + B) + \sin(A - B) \tag{C.1a}$$
$$\sin^-(A \pm B) = \sin(A + B) - \sin(A - B) \tag{C.1b}$$

and the equivalent for cos; the terms are written in this expanded form to make the frequency content of the responses explicit. This leads to the following equations:
Surge:

$$\ddot\alpha + p_f^2\alpha = A\lambda\omega^2 \sin\omega t \tag{C.2a}$$
$$\ddot\beta + p_e^2\beta = g\lambda \sin\Omega t \tag{C.2b}$$

Sway: see results for heave below, as before.
Heave:

$$\ddot\alpha + p_f^2\alpha = -\frac{A\lambda}{2}\omega^2\alpha \sin^-(\omega \pm \Omega)t \tag{C.3a}$$
$$\ddot\beta + p_e^2\beta = \frac{A\lambda}{2}\omega^2\left[\cos^-(\omega \pm \Omega)t - \beta\sin^-(\omega \pm \Omega)t\right] + g\lambda\sin\Omega t \tag{C.3b}$$

Roll:

$$\ddot\alpha + p_f^2\alpha = \alpha\left(\frac{A\omega}{2}\right)\left[-4\Omega\cos\omega t + \lambda(g + h\omega^2)\cos^-(\omega \pm \Omega)t\right]$$
$$- \alpha\left(\frac{A\omega}{2}\right)^2\left[2 + 2\cos 2\omega t + 2h\lambda\cos\Omega t\right.$$
$$\left. + h\lambda\cos^+(2\omega \pm \Omega)t\right] \tag{C.4a}$$
$$\ddot\beta + p_e^2\beta = g\lambda\sin\Omega t + A\omega^2\sin\omega t$$
$$+ \frac{A\lambda}{2}(g + h\omega^2)\left[\sin^-(\omega \pm \Omega)t + \beta\cos^-(\omega \pm \Omega)t\right]$$
$$- \left(\frac{A\omega}{2}\right)^2 h\lambda\left[\sin^-(2\omega \pm \Omega)t + \beta\cos^+(2\omega \pm \Omega)t\right.$$
$$\left. + 2\sin\Omega t + 2\beta\cos\Omega t\right] \tag{C.4b}$$

Pitch:

$$\ddot{\alpha} + p_f^2 \alpha = A\lambda \left(g + h\omega^2\right) \sin \omega t$$

$$+ \left(\frac{A\omega}{2}\right) \left[(\omega + 2\Omega) \sin(\omega + \Omega)t + (\omega - 2\Omega) \sin(\omega - \Omega)t\right]$$

$$- \alpha \left(\frac{A\omega}{2}\right)^2 \left[2\lambda h \cos \Omega t + \lambda h \cos^+(2\omega \pm \Omega)t\right.$$

$$+ \cos 2\Omega t + \frac{1}{2} \cos^+(2\omega \pm 2\Omega)t$$

$$\left. - 1 - \cos 2\omega t\right] \tag{C.5a}$$

$$\ddot{\beta} + p_e^2 \beta = g\lambda \sin(\Omega t)$$

$$- \left(\frac{A\omega}{2}\right)^2 \left\{2h\lambda \left[\sin \Omega t + \beta \cos \Omega t\right] + \left[\sin 2\Omega t + 2\beta \cos 2\Omega t\right]\right.$$

$$+ h\lambda \left[\sin^-(2\omega \pm \Omega)t + \beta \cos^+(2\omega \pm \Omega)t\right]$$

$$\left. + \frac{1}{2} \sin^-(2\omega \pm 2\Omega)t + \beta \cos^+(2\omega \pm 2\Omega)t\right\}$$

$$\tag{C.5b}$$

Yaw:

$$\ddot{\alpha} + p_f^2 \alpha = -\left(\frac{A\omega}{2}\right) \left[(\omega + 2\Omega) \cos(\omega + \Omega)t - (\omega - 2\Omega) \cos(\omega - \Omega)t\right]$$

$$+ \alpha \left(\frac{A\omega}{2}\right)^2 \left[1 + \cos 2\Omega t + \cos 2\omega t + \frac{1}{2} \cos^+(2\omega \pm 2\Omega)t\right] \tag{C.6a}$$

$$\ddot{\beta} + p_e^2 \beta = g\lambda \sin \Omega t$$

$$+ \left(\frac{A\omega}{2}\right)^2 \left[\frac{1}{2} \sin^-(2\omega \pm 2\Omega)t + \beta \cos^+(2\omega \pm 2\Omega)t\right.$$

$$\left. + \sin 2\Omega t + 2\beta \cos 2\Omega t\right] \tag{C.6b}$$